Electrochimica Acta 153 (2015) 149–158

Contents lists available at ScienceDirect

Electrochimica Acta

journal homepage: www.elsevier.com/locate/electacta

The behavior of dissolution/passivation and the transformation of passive films during electrocoagulation: Influences of initial pH, Cr(VI) concentration, and alternating pulsed current

Zhao-hui Yang [a,b,*], Hai-yin Xu [a,b], Guang-ming Zeng [a,b], Yuan-ling Luo [a,b], Xia Yang [a,b], Jing Huang [a,b], Li-ke Wang [a,b], Pei-pei Song [a,b]

[a] College of Environmental Science and Engineering, Hunan University, Changsha 410082, P.R. China
[b] Key Laboratory of Environmental Biology and Pollution Control (Hunan University), Ministry of Education, Changsha 410082, P.R. China

ARTICLE INFO

Article history:
Received 8 May 2014
Received in revised form 27 November 2014
Accepted 27 November 2014
Available online 29 November 2014

Keywords:
alternating pulsed current
electrocoagulation
Cr(VI) concentration
dissolution
passivation

ABSTRACT

The passivation behavior of an iron anode for electrocoagulation (EC) was first investigated using response surface methodology (RSM). Tested initial pH range, Cr(VI) concentration and alternating pulsed current (APC) were 4.0 to 8.0, 52 to 520 mg L^{-1} and 10 to 590 s, respectively. The distance between electrodes was 25 mm, and K_2SO_4 (1 g L^{-1}) was used as the supporting electrolyte in a 2.5 L EC reactor. Results confirmed that initial pH, Cr(VI) concentration, and APC significantly influence the extent of passivation. Then, based on the interaction effect on passivation behavior between initial pH and Cr(VI) in RSM, a pH-Cr(VI)-dissolution/passivation diagram was constructed with galvanostatic measurements. The diagram showed an optimal dissolution region for EC operation. This optimum was characterized by a reasonable final pH for extended precipitation and little passivation. Results of the cyclic voltammetry and X-ray photoelectron spectroscopy revealed a significant difference in the composition and stability of oxide films in the region with more pronounced passivation. Interestingly, the APC had both positive and negative effect on the passivation behavior. Long period of APC (T_{APC} = 590 s) produced a non-protective film, which favored the Fe^0 dissolution. However, a more stable and protective passive film with a uniform structure of Fe and Cr oxides was formed by short T_{APC} (10 s). Based on the above results, this study elucidated the behavior of dissolution/passivation and the transformation of passive films during the Fe-EC process for Cr(VI) treatment.

1. Introduction

Over the past decade, electrocoagulation (EC) has gained recognition as an effective technology of removing Cr(VI) [1–5]. During the EC process, active Fe(II)-coagulant species, which are generated *in situ* by the electrochemical dissolution of a sacrificial iron anode [6,7], reduce Cr(VI) to Cr(III) [5,8]. Consequently, a pH increase to more alkaline conditions is observed [5], initiating further spontaneous reactions, involving the product metal ions (Fe(III) and Cr(III)), which produce corresponding hydroxides and/or polyhydroxides [9]. The newly formed iron/chromium precipitates can then be separated from the treated water by flotation with small hydrogen bubbles (diameter ranged from 17 μm to 50 μm) that are electrolytically generated from the cathode [1,4]. Recent studies have shown that the hydrogen recovered from the EC process could offset operational costs because of its value as a green energy source [10,11].

As a technique used for wastewater treatment, EC evidently exhibits great promise; yet, its application is hampered by passivation issues. In particular, the formation of an inhibiting layer on the electrode, usually an oxide, prevents the continuous iron dissolution and electron transfer, thereby decreasing the efficiency of Cr(VI) removal [2,3,8,12]. Passivation induces a significant increase in the passive over potential, resulting in higher power consumption [13]. Moreover, the oxygen evolution reaction is thermodynamically spontaneous at the anode under passivation conditions, limiting the recovery of hydrogen [8,11].

Passivation is widely observed by many authors during the Fe-EC process for Cr(VI) removal [3,5,8,12,14–16]. Generally, two major ways have been chosen to solve this problem.

The first is by adding sufficient or superfluous chloride ions to breakdown the formed passive film to improve the efficient of Cr

* Corresponding author. Tel.: +86 15717484818; fax: +86 0731 88822829.
E-mail address: yzh@hnu.edu.cn (Z.-h. Yang).

http://dx.doi.org/10.1016/j.electacta.2014.11.183
0013-4686/

(VI) removal, which is an "end-treatment" method. Therefore, a question might be introduced if the passivation could be inhibited from the original by adjusting some factors?

To deal with this question, understanding the behavior of dissolution/passivation of passive film is very important. However, crucial knowledge about the formation of passive films in Fe^0-EC systems for Cr(VI) removal is lacking.

Fortunately, the corrosion and passivation process has been largely investigated in Fe^0/H_2O systems.[17–21] For example, Sato et al. [18,21] considered that the corrosion process in Fe^0/H_2O system involves the electrochemical and acid-base reactions, and the passivation is induced by the hydroxide-catalyzed mechanism of metal dissolution. And Cohen et al. [19] suggested that the passive film is formed first by the oxidation of water-formed magnetite and then further thickened by the oxidation of diffusing Fe^{2+}. The formation of passive films is formed by the action of chromate inhibition.[20]

In addition, Nesic et al. [22] proposed a theory about the formation of iron carbonate scales/films in a CO_2 corrosion system, and they considered that the growth and protectiveness of these scales/films depend on the relative kinetics of iron corrosion (dissolution) and precipitation (oxide film formation). When the rate of precipitation at the steel surface exceeds the rate of corrosion, dense protective scales form [23]. These protective scales are sometimes very thin, but still protective [24]. These provide some references for our study, due to the Fe-EC system can be essentially considered as an electrochemically ($U_0 \neq 0$) driven accelerated corrosion process [9,25].

As shown in Table 1, the process of Fe-EC removing Cr(VI) is complex with a multitude of reactions, including the dissolution (chemical dissolution and electrodissolution) [26,27], reduction (cathode reduction and zero iron reduction process) [8,28,29] and precipitation [5,8,16,25]. Therefore, it is reasonable to assume that the factors which affecting the kinetics of dissolution, reduction and precipitation may influence the formation of passive films in Fe-EC process.

Specifically, pH could directly influence the corrosion (Eq. (2)) [26] and reduction (Eq. (3–4)) [8,28,29] and precipitation rates (Eq. (5–7)) [5,25]. High pH favors the precipitation process (Eq. (5–7)), but inhibits the chemical dissolution (Eq. (2)). For Cr (VI), as an effective inhibitor of Fe corrosion, would gather to the surrounding of anode under the effect of electric field, and then promote the chemical reduction and the Cr(VI) reduction by Fe^0 (Eq. (3–4)). While current density theoretically quantifies the rate of iron that is dissolved from the anode. From the above, it is possible by adjusting the Cr(VI), pH and current density to inhibit the occurrence of passivation.

The second way to prevent the passivation is by alternating pulsed current (APC) in EC process [16,30]. Considerable researches documented that APC is efficient in preventing the passivation in Al electrodes by the transformation of passive film formed in Al-EC process [31,32]. Similar analyses conducted during the Fe-EC system indicated that APC is also effective in preventing Fe-passivation [16,30]. These experiments, however, were performed with chloride, which is well known as a depassivation agent. Thus, clearly distinguishing the cause of depassivation might be difficult. By contrary, APC is reported to improve the stability of passive film on stainless steel [33,34].

Thus, to investigate the influence of APC on Cr(VI) removal during EC process, it is necessary to know the transformation of the passive film.

Above all, understanding the behavior of dissolution/passivation and the transformation of passive films is crucial for the successful application of Fe-EC in removing Cr(VI). In this study, the underlying effects of the above mentioned factors on iron passivation during the EC process are assessed with the response surface methodology (RSM). Following the confirmation of the influencing factors, the dissolution/passivation region is determined, and the means of how these influencing factors affect the passive film composition and stability are investigated. Subsequently, the behavior of dissolution/passivation and the transformation of passive films during the Fe-EC process for Cr(VI) wastewater treatment are elucidated.

2. Experimental

2.1. Electrocoagulation experiments

2.1.1. Experimental set-up

Experiments were conducted in a 2.5 L EC reactor, as described previously [5], using reagent-grade iron rod (99.5% Fe) with active surface area of 20 cm^2. The distance between the anode and cathode was 25 mm. The electrodes, precleaned mechanically with 800 grit SiC papers to remove any passive film, were connected to a programmable DC power supply (RIGOL DP1116A, China, maximum 32.000 V and 10.000 A) which controlled by user-

Table 1
Relevant reactions of dissolution and precipitation during EC process.

Processes		Equations	
Dissolution kinetics (ν_d)	Electro -dissolution	$Fe - 2e^- =^{\nu_2} Fe^{2+}$ $\nu_2 = d[Fe(II)]/dt = i \cdot A/(n \cdot F \cdot V)$	(1)
	Chemical dissolution	$Fe + 2H^+ =^{\nu_1} Fe^{2+} + H_2(g)$ $\nu_1 = d[Fe(II)]/dt = f(pH, A)$	(2)
Reduction & precipitation kinetics (ν_p)	Chemical reduction	$3Fe(II) + Cr(VI) =^{\nu_3} 3Fe(III) + Cr(III)$ $\nu_3 = -d[Fe(II)]/dt = k_3[Fe(II)][Cr(VI)]$	(3)
	Cr(VI) reduction by Fe^0	$Fe + Cr(VI) =^{\nu_4} Fe(III) + Cr(III)$ $\nu_4 = -d[Fe(II)]/dt = k_4[Cr(VI)]^{0.5}[H^+]^{0.5}A$	(4)
	Fe(II) precipitation	$Fe^{2+} + 2OH^- \overset{Ksp_1}{\rightleftharpoons} Fe(OH)_2(S); pKsp_1 = 15.1$	(5)
	Fe(III) precipitation	$Fe^{3+} + 3OH^- \overset{Ksp_2}{\rightleftharpoons} Fe(OH)_3(S); pKsp_2 = 37.4$	(6)
	Cr(III) precipitation	$Cr^{3+} + 3OH^- \overset{Ksp_3}{\rightleftharpoons} Cr(OH)_3(S); pKsp_3 = 30.2$	(7)

where A is surface area, k_3 and k_4 are the rate coefficient, K_{sp} is solubility product.

defined programming. A programmable time relay (JSPG–120–B, China) was used to obtain the alternating pulsed current and adjust the period of APC [31]. Each run was conditioned for 60 min with current density 100 A m^{-2}. Synthetic solutions containing Cr (VI) were prepared by dissolving reagent grade $K_2Cr_2O_7$ into ultrapure water, and the K_2SO_4 with the concentration of 1 g L^{-1} was used as the supporting electrolyte. The pH of the solutions was adjusted by adding 0.5 M NaOH or H_2SO_4 solutions and measured by pH meter (FE20, METTLER TOLEDO, Switzerland). A faster stirring rate of 600 rpm was used during the electrolysis to eliminate mass transfer effect [30]. All experiments were conducted at room temperature (23 ± 2 °C). Fe(Tot) concentrations were analyzed using flame atomic absorption spectroscopy (AAS).

2.1.2. RSM experimental design

Some single-factor experiments were performed to obtain an appropriate range of selected factors (initial pH, Cr(VI) concentration, current density and period of APC) before the assessment of underlying effects of the above mentioned factors on iron passivation by RSM [35].

The Box-Behnken Design, a standard RSM, was selected to evaluate the influence of three selected factors (initial pH (x_1), Cr (VI) concentration (x_2), and the period of APC (x_3)) on the current efficiency (y) during Cr(VI) removal in Fe-EC process. All factors were controlled at three levels. The response variable (y) that represented current efficiency was fitted by a second-order model in the form of quadratic polynomial equation:

$$y = \beta_0 + \sum_{i=1}^{m} \beta_i X_i + \sum_{i<1}^{m} \beta_{ij} X_i X_j + \sum_{i=1}^{m} \beta_{ii} X_i^2 \quad (8)$$

where y is the response variable to be modeled. x_i and x_j are independent variables which determine y. β_0,β_i and β_{ii} are the offset term, the linear coefficient and the quadratic coefficient, respectively. β_{ij} is the term that reflect the interaction between x_i and x_j.

2.1.3. Calculation of current efficiency

The current efficiency (Φ) was defined as the ratio of the actual dissolved iron (Δm_{exp}) to the theoretical value which due to the passage of electrical charge in a volume of water calculated using Faraday's law (Δm_{theo}):

$$\Phi = \frac{\Delta m_{exp}}{\Delta m_{theo}} = \frac{Fe(Tot)\cdot V\cdot n\cdot F}{0.1\cdot M\cdot i\cdot A\cdot t}\cdot 100\% \quad (9)$$

where *Fe(Tot)* is the concentration of dissolved iron (mg L^{-1}), V is the volume of water (2.5 L), t is the time of electrolysis (3600 s), M is the atomic weight of the iron (56 g mol^{-1}), i is the current density (100 A m^{-2}), A is the surface area of anode (20 cm^2), n is the number of electron moles (n = 2, in Eq. (1)) and F is the Faraday's constant (F = 96,487C mol^{-1}).

2.2. Electrochemical experiments

2.2.1. Electrochemical cell and electrode preparation

Electrochemical measurements were carried out on electrochemical work station (CHI 760E, china) with a standard three-electrode cell. The working electrode was made of pure iron disc (99.9%) which was embedded in resin with an exposed area of 8.3 mm^2. A large-area platinum electrode was employed as counter electrode and an Hg/Hg_2SO_4 (saturated K_2SO_4) reference electrode as the reference electrode, which was connected to the cell through a Luggin capillary, whose tip was set at a distance of about 1 mm from the surface of the working electrodes to minimize the variations due to iR-drop in the electrolyte. Prior to each experiment, unless specified otherwise, the working electrode was polished manually with 800 grit SiC papers, followed by alumina polishing to a 0.3 μm wet finish, and sonicated in an ethanol for 5 min to remove polishing residues. Solutions were deaerated by N_2 for 30 min before use. All potentials were quoted on the Hg/Hg_2SO_4 scale (0.418 V vs. SCE, 0.659 V vs. SHE).

2.2.2. Galvanostatic measurements

Galvanostatic measurements were performed to determine the dissolution/passivation region affected by the interaction term of initial pH (2 to 8) and Cr(VI) concentration (52 to 520 mg L^{-1}). A constant current of 8.3E–4 A (ca. 100 A m^{-2}) was applied for 300 s (which is identical to all subsequent time) during each experiment and the electrode potential was recorded as a function of time. A typical schematic diagram of time dependence of electrode potential corresponds to dissolution and passivation behavior was shown in Fig. 1. It could be seem that, the constant potential value, above the reversible potential of oxygen evolution, was indicative of the occurrence of passivation. Otherwise, the potential between the reversible potential of oxygen evolution and hydrogen evolution indicated the dissolution of iron.

2.2.3. Chronopotentiometry

Chronopotentiometry was used to form the passive film of EC process, in which the operational parameters (current density = 100 A m^{-2}, reaction time = 60 min, stirring rate = 600 rpm) were equipped identically to that in EC reactor. Chronopotentiometry experiments were performed with direct current and APC conditions respectively. At direct current model, the passive films were formed in three different conditions: pH 4 and Cr(VI) = 520 mg L^{-1}, pH 8 and Cr(VI) = 520 mg L^{-1} and pH 8 and Cr(VI) = 52 mg L^{-1}. At APC model, the experiments were performed in the condition of pH 4 and Cr(VI) = 520 mg L^{-1}, while the period of square wave was set at 10 s and 590 s, respectively.

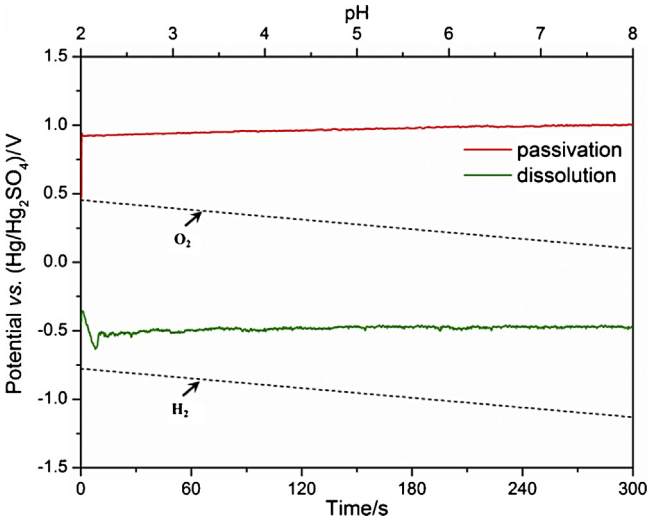

Fig. 1. Schematic diagram of time dependence of electrode potential correspond to passivation and dissolution behavior.

Table 2
Parameters for deconvolution of XPS spectra.

Element	Chemical state	Binding energy (eV)	FWHM (eV)	G/L
Fe (2p3/2)	Fe^0 (met)	706.8	1.80	0.8
	Fe^{2+} (ox)	709.5	1.95	
	Fe^{3+} (ox)	711.2	2.60	
	Fe^{3+} (hyd)	713.2	3.00	
Cr (2p3/2)	Cr^0 (met)	574.1	1.38	0.8
	Cr^{3+} (oxi)	576.4	1.93	
	Cr^{3+} (hyd)	577.6	2.06	
O (1s)	O^{2-} (oxi)	530.1	1.71	0.8
	OH^- (hyd)	531.7	2.00	
	O^{2-} (H_2O)	533.3	1.56	

2.2.4. Cyclic voltammograms (CVs)

The treated samples by chronopotentiometry were rinsed with ultrapure water before the electrochemical characterization of the passive films was studied by CVs. All the experiments were performed in borate buffer with a pH value of 8.4 (0.075 M $Na_2B_4O_7{\cdot}10H_2O$, 0.3 M H_3BO_3) at a sweep rate of 10 mV s^{-1}.

2.2.5. Surface analysis

The treated samples by chronopotentiometry was dried and preserved with N_2 for X-ray photoelectron spectroscopy (XPS) analysis, which performed on a ESCALAB 250Xi X-ray photoelectron spectrometer (Thermofisher Scientific, USA) with an incident X-ray energy of 1486.8 eV (Al Ka) operated at 13 kV and 200 W under residual pressure of 10^{-9} Torr. Depth profiling was achieved by argon ion bombardment with ion energy of 3 keV. The sputtering rate was about 2 nm min^{-1} for SiO_2. The measured sample current density during depth profiling was 120 μA cm^{-2}, and the bombardment area was 3.25 mm in diameter. The core-level spectra for films were obtained at take-off angles of 45°. Data analysis involved smoothing, non–linear Shirley-type background subtraction and curve fitting using mixed Gaussian-Lorentzian functions. Spectral bands were deconvoluted into peaks with the software XPSPEAK using an integrated background subtraction (Table 2) [36]. The binding energy was corrected for charging effects by referencing to the C1s peak (284.8 eV).

3. Results and discussion

3.1. Significant factors for passivation in EC process

3.1.1. Determining the range of selected factors for RSM

In the Fe-EC process, the current efficiency is generally around 100% without passivation. However, if passivation occurs, a part of the current will be wasted to produce O_2 as a consequence of passive film formed on the surface of electrode [14]. Accordingly, a decrease of current efficiency will be observed. Therefore, the current efficiency can be used as an index to reflect the extent of passivation.

In order to improve the significance of the fitted model, an appropriate range of selected factors is essentially important in RSM experiments [35]. Thus, some single-factor experiments were performed in this study prior to designing the RSM (Fig. 2). The figure specifies that initial pH, Cr(VI) concentration, and APC significantly affected the current efficiency. By contrary, the corresponding current efficiency of the current density was essentially unchanged (only 4.7% fluctuation) in the range of 25 A m^{-2} to 250 A m^{-2} (Fig. 2). Therefore, the current density was not selected as an influencing factor for the RSM design. In this event, all experiments were performed under a fixed current density condition with 100 A m^{-2}.

Many reports proposed that the period of APC (T_{APC}) at 900 s to 1800 s is effective for depassivation in the Fe-EC process [2,30]. However, Keshmirizadeh et al. [16] also proposed that even a shorter T_{APC} with 480 s could have a conducive effect on depassivation. This study investigated the effect of continuously decreasing T_{APC} on depassivation by setting the minimum of T_{APC} at 10 s. The results indicated that APC displayed litter effect on the current efficiency when the T_{APC} was higher than 590 s (Fig. 2). Thus, the coded levels of T_{APC} for RSM were selected from the range of 10 s to 590 s. Similar methods were also adopted to determine the ranges of initial pH and Cr(VI) concentration, and the results are exhibited in Table 3.

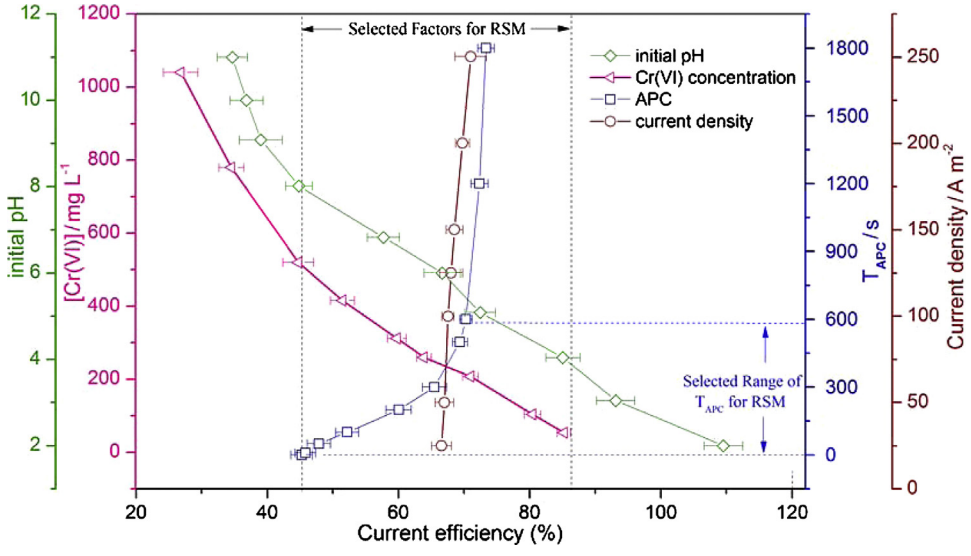

Fig. 2. Effect of selected factors (initial pH, Cr(VI) concentration, APC and current density) on current efficiency. Conditions: (1) for initial pH experiment, Cr(VI) = 260 mg L^{-1}, T_{APC} = 300 s, current density = 100 A m^{-2}; (2) for Cr(VI) concentration experiment, initial pH = 6, T_{APC} = 300 s, current density = 100 A m^{-2}; (3) for APC experiment, initial pH = 6, Cr(VI) = 260 mg L^{-1}, current density = 100 A m^{-2}; (4) for current density experiment, initial pH = 6, Cr(VI) = 260 mg L^{-1}, T_{APC} = 300 s.

Table 3
Coded levels of 3 variables for BBD framed by single-factor experiments.

Factors	Codes	Coded levels		
		−1	0	+1
Initial pH	x_1	4	6	8
Cr(VI) (mg L^{-1})	x_2	52	286	520
T_{APC} (s)	x_3	10	300	590

3.1.2. Experimental results of RSM

Table 4 shows the experimental matrices of initial pH (x_1), Cr(VI) concentration (x_2), and T_{APC}(x_3) and the corresponding experimental response. The variance (ANOVA) of response surface quadratic model was analyzed, in which the results revealed that the model was highly significant (F-value 58.92, "Prob >F" less than 0.0001) with insignificant *lack of fit* (F-value 5.64, "Prob >F" 0.0641). This conclusion depicts that this model is acceptable to analyze the factors [37]. The pareto chart was used to determine which factors (x_1, x_2, x_3) significantly influenced the response variable (y). The length of each bar in the chart is proportional to the absolute value of its associated estimated effect on the response. A vertical line (reference line) was drawn at the location of the $P = 0.05$ critical value [38]. Any bars that extend to the right of that line indicated that the effects were statistically significant at the 5% significance level. Fig. 3 illustrates that the terms x_2, x_1, x_1x_2, x_2x_2, x_3, and x_1x_1, which extend behind the reference line, remarkably affected the current efficiency yield (y) in order of their influences. This finding confirmed that the three factors, namely, the initial pH, Cr(VI) concentration, and APC can all affect passivation during the EC process. Among all factors, the negative terms x_2, x_1, x_1x_1, and x_2x_2 demonstrated an unfavorable effect on the current efficiency, promoting the formation of passive film. By contrary, the positive term x_3 showed a favorable effect to arrest passivation.

The current efficiency decreased with the increase of Cr(VI) concentration and initial pH, as shown in Fig. 4. In particular, the current efficiency decreased to approximately 40% with high Cr (VI) (blue region), suggesting that passivation occurred. By contrary, the current efficiency was nearly 100% with low pH and Cr(VI) (red region), emphasizing that the passivation of iron did not occur.

3.2. Dissolution/passivation region in Fe-EC process

The quantitative relevance of the initial pH and Cr(VI) concentration was examined by constructing a dissolution/passivation region diagram (Fig. 5) with galvanostatic measurements. The green line is the border of dissolution and passivation. Regions I and II, which are located below the green line, indicated that the dissolution of iron was observed. Conversely, Region III above the green line specified that passivation occurred.

The occurrence of dissolution or passivation depended on the relative kinetics of iron dissolution process (ν_d) (Eqs. (1 to 2)) [24,25,39] and its reduction (Eqs. (3 to 4)) and precipitation process (ν_p) (Eqs. (5 to 7)) [5,28,29,39], which are involved in the Fe-EC process (Table 1).

According to the Nesic et al., when $\nu_d > \nu_p$, no passivation occurs; otherwise, passivation ensues [22]. Therefore, ν_d was supposed $> \nu_p$ in the dissolution Regions I and II, whereas ν_d was $< \nu_p$ in the passivation Region III. In the green line, $\nu_d = \nu_p$. When the amount of Cr(VI) was increased, the reduction and precipitation rate increased according to Eqs. (3 to 4). Thus, the equivalence of ν_d and ν_p can be maintained by simultaneously decreasing the pH value (Eq. (2)).

Additionally, the solubility of Cr(III) is a function of pH. Approximately 50% Cr(III) remained dissolved in the solution at pH 4.5, whereas no precipitation of $Cr(OH)_3$(s) was formed at pH 4 (Eq. (7)) [5]. Thus, controlling the final pH in neural or alkaline conditions might be beneficial in removing Cr (III) from the EC process to enhance its precipitation as Cr $(OH)_3$(s). Specifically, as discussed in our previous study [5], when $p[Cr(VI)] = pH_i$, the final pH is neutral; $p[Cr(VI)] < pH_i$, alkaline; and $p[Cr(VI)] > pH_i$, acidic. Therefore, the final pH that corresponded to Regions II and III was alkaline, and that in Region I was acidic. So, it was worth to emphasize that Region II was the optimal conditions for EC operation because it achieved a reasonable final pH for precipitation and did not suffer passivation.

Table 4
Experimental matrix for natural variables and corresponding experimental response to Current efficiency.

Run no.	Std no.	Initial pH	Cr(VI) (mg L^{-1})	T_{APC} (s)	Current efficiency (%)
1	15	6.00	286.00	300	70.4
2	7	4.00	286.00	590	80.4
3	9	6.00	52.00	10	84.3
4	10	6.00	520.00	10	28.6
5	17	6.00	286.00	300	67.8
6	14	6.00	286.00	300	65
7	2	8.00	52.00	300	60.7
8	8	8.00	286.00	590	55.3
9	3	4.00	520.00	300	40.2
10	1	4.00	52.00	300	94.1
11	11	6.00	52.00	590	89.6
12	5	4.00	286.00	10	65.5
13	16	6.00	286.00	300	68.3
14	13	6.00	286.00	300	67.8
15	12	6.00	520.00	590	41
16	6	8.00	286.00	10	48.9
17	4	8.00	520.00	300	32.4

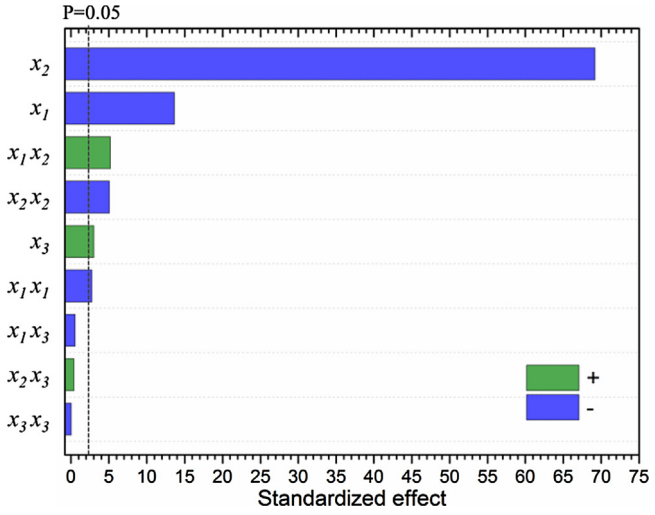

Fig. 3. Pareto chart of standardized effects for the model of the current efficiency. The line indicates the 95% confidence level, and factors with standardized effect values to the right of this line are statistically significant.

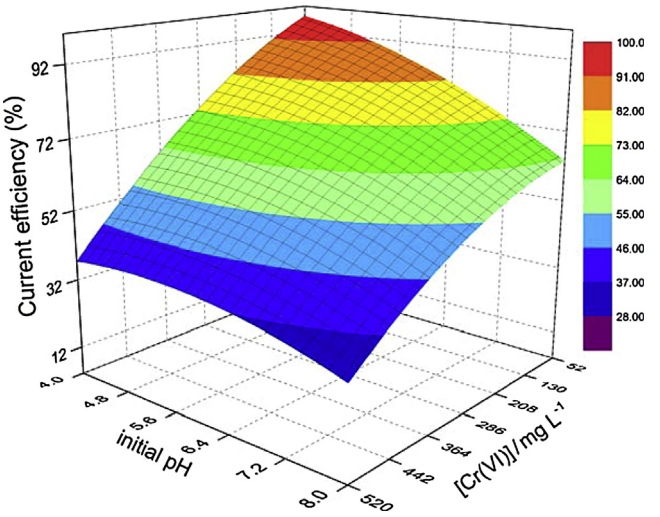

Fig. 4. Surface response to the quadratic experimental design of the current efficiency (y) as the function of initial pH (x_1) and Cr(VI) concentration (x_2).

3.3. Cyclic voltammetry (CVs)

CV experiments were performed to investigate the transformation of passive film, which was formed in the Fe-EC process. In Fig. 6a, the anodic reversal potential is below the transpassive dissolution region of Cr(III) oxide (0.336 V *vs* Hg/Hg_2SO_4) [40,41]. For the pH 8 and Cr(VI) = 52 mg L^{-1} sample, two cathodic peaks (I and II) were assigned to the electrochemical reactions 10 and 11, respectively [42,43]. Hence, the passive film that consists of Fe $(OH)_3$ and Fe_3O_4/Fe_2O_3 can be reduced to Fe^{2+} or FeO. Under a more negative potential (−1.37 V *vs.* Hg/Hg_2SO_4), iron oxide can be reduced to metallic Fe^0 with a larger reduction time [42].

$$Fe(OH)_3(s) + 1e^- = Fe^{2+}(aq) + 3OH^-(aq) \quad (10)$$

$$Fe_3O_4/Fe_2O_3(s) + 4H^+ + 4e^-(aq) = 5FeO(s) + 2H_2O \quad (11)$$

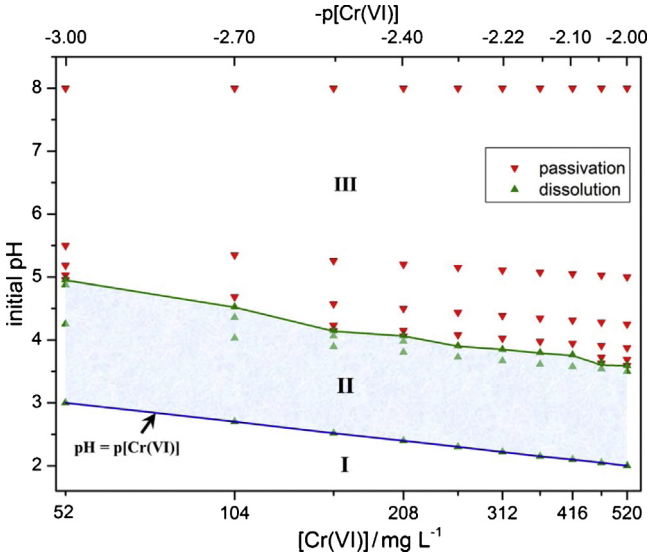

Fig. 5. Region of dissolution and passivation under different initial pH and Cr(VI) concentration (or −p[Cr(VI)]) conditions. The blue line corresponds to final pH = 7.0. The green line is the borders of dissolution and passivation.

The subsequent anodic peak III in the active–passive region was assigned to reaction 12, which was the predominant procedure of iron dissolution in the EC process. If the solution is basic, the product of Fe(II) can further react with OH^- (Eq. (13)).

$$Fe^{(0)}(s) = Fe^{2+}(aq) + 2e^- \quad (12)$$

$$Fe^{(0)}(s) + 2OH^-(aq) = Fe(OH)_2(s) + 2e^- \quad (13)$$

Peak V was registered at −0.58 V *vs.* Hg/Hg_2SO_4. This condition indicated the formation of Fe(III), which contained compounds such as Fe_3O_4 ($FeO{\cdot}Fe_2O_3$) [44].

For the pH 8 and Cr(VI) = 520 mg L^{-1} and pH 4 and Cr (VI) = 520 mg L^{-1} samples, the same peak III was observed, but with a dramatic decrease in intensity. This finding signified that in such cases, the stability of passive film increases. Meanwhile, the passive film showed an anodic peak IV at −0.8 V *vs.* Hg/Hg_2SO_4 that was attributed to the Fe(III) oxide formation on the surface by reaction 14 [42,45].

$$2Fe(OH)_2 = Fe_2O_3 + H_2O + 2H^+ + 2e^- \quad (14)$$

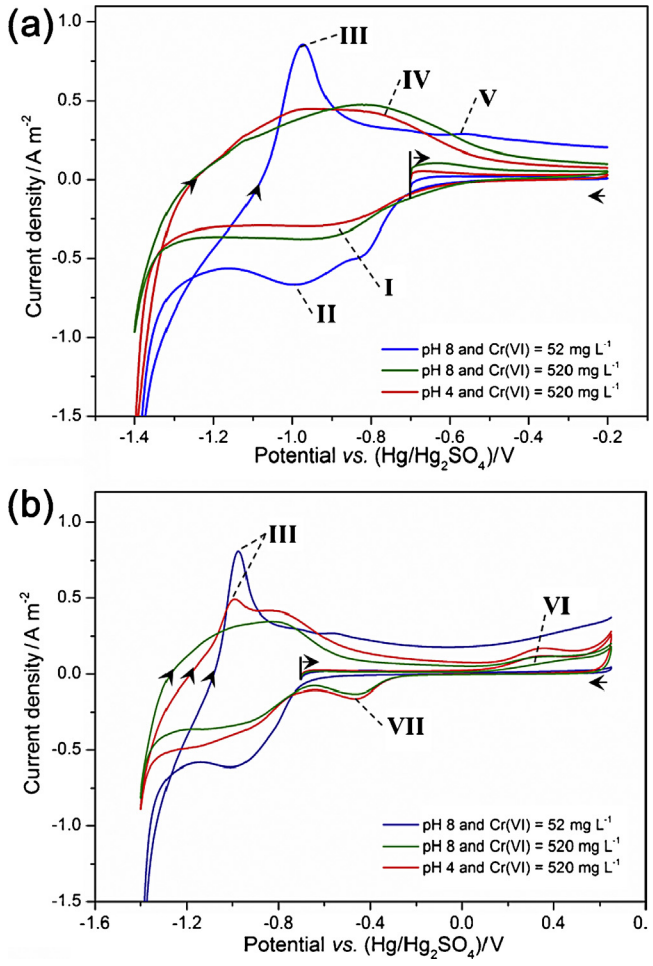

Fig. 6. Comparison of the CVs of passive film in pH 8.4, borate–buffer solutions treated with different initial pH and Cr(VI) concentrations at direct current model: (a)−0.7 → − 0.2 → − 1.4 → − 0.2, (b)−0.7 → + 0.65 → − 1.4 → + 0.65.

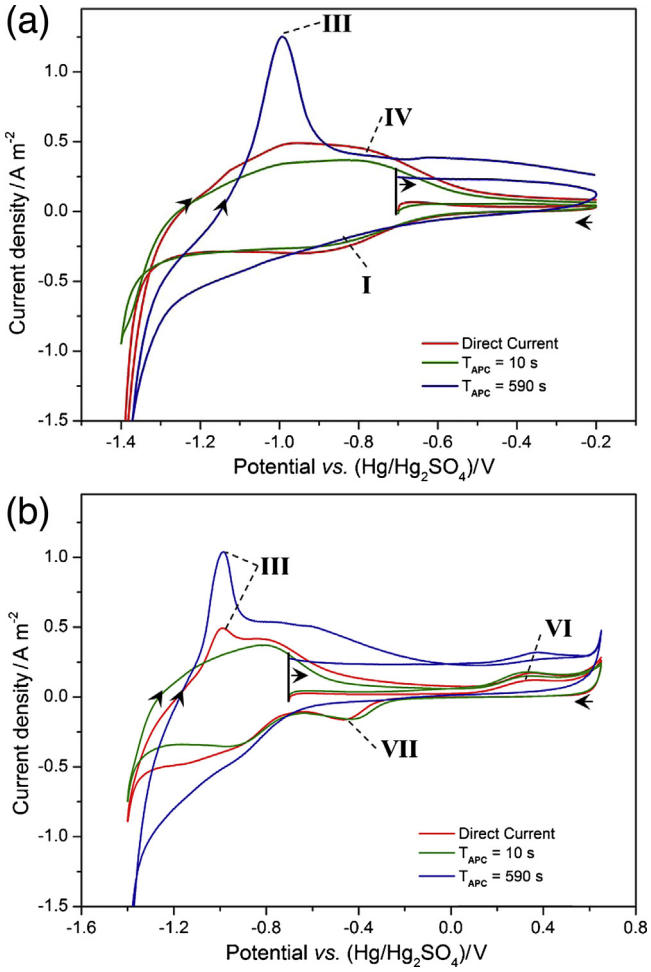

Fig. 7. Comparison of the CVs of passive film in pH 8.4, borate–buffer solutions treated with different ACP conditions at pH = 4 & Cr(VI) concentration = 520 mg/L: (a)–0.7 → – 0.2 → – 1.4 → – 0.2, (b)–0.7 → + 0.65 → – 1.4 → + 0.65.

The formation of passive film might be accompanied by reaction 15 and 16 in this process [40,41,46].

$$2Fe \cdot H_2O_{ads} + 2CrO_4^{2-} = Fe_2O_3 + Cr_2O_3 + 4OH^- \quad (15)$$

$$6Fe^{2+} + 2CrO_4^{2-} + 4H_2O = 3Fe_2O_3 + Cr_2O_3 + 8H^+ \quad (16)$$

When the potential increased to 0.336 V *vs.* Hg/Hg_2SO_4 (Fig. 6b), an anodic peak VI, which was assigned to the oxide of Cr(III), was detected (Eq. (17)) [40].

$$Cr_2O_3 + 5H_2O = CrO_4^{2-} + 6H^+ + 6e^- \quad (17)$$

The oxygen evolution reaction ultimately occurred with a sustained increase in potential, which is the feature of passivation occurrence and results in a decreasing of current efficiency.

The results of this study further revealed that the samples with pH 8 and Cr(VI) = 52 mg L^{-1} contained insufficient chromium oxide and reduction peak, suggesting that the formed passive film consisted of trace amount of Cr(III) oxide. This interesting phenomenon is constructed with the subsequent interpretations. First, the formation of passive film involved in Cr is thermodynamically spontaneous, including the two major routes (Eq. (15 to 16)) [40,41,46]. In theory, the ratios of Cr/(Cr + Fe) in passive film were between 25% (all produced by Eq. (16)) to 50% (all produced by Eq. (15)). Then, the potential in the case of passivation was higher than the Cr(III) oxidation (0.336 V *vs.* Hg/Hg_2SO_4), as denoted in Fig. 1, resulting in the dissolution of Cr(III) oxide (Eq. (17)).

For the pH 8 and Cr(VI) = 520 mg L^{-1} and pH 4 and Cr (VI) = 520 mg L^{-1} samples, two peaks (VI and VII) that correspond to the oxidation–reduction processes of Cr were observed [40,41,45]. In the first anodic sweep (peak VI), Cr(III) initially was oxidized to Cr(VI), which subsequently reduced back to Cr(III) in the second cathodic sweep (peak VII). This circumstance implied that some Cr species were incorporated in the oxide layer [41,47].

As previously discussed, peak III responded to the iron dissolution, which is an indicator of the stability of passive film. In particular, when the intensity in peak III was higher, the passive film was more unstable. Thus, the stabilities of the passive film in the above cases are as follows: pH 8 and Cr(VI) = 520 mg L^{-1} > pH 4 and Cr(VI) = 520 mg L^{-1} > pH 8 and Cr(VI) = 52 mg L^{-1}.

In comparison with a direct current sample, T_{APC} with 590 s showed a dramatically higher intensity in peak III (Fig. 7a), signifying that a more unstable film was obtained. Moreover, the T_{APC} demonstrated a peak (VI) that corresponded to the oxidation of Cr(III), but with the absence of the chromate reduction peak (VII) (Fig. 7b). This situation suggests that chromate species were not incorporated in the oxide layer. Therefore, this study inferred that a longer T_{APC} (T_{APC} = 590 s) strategy generated a non-protective and

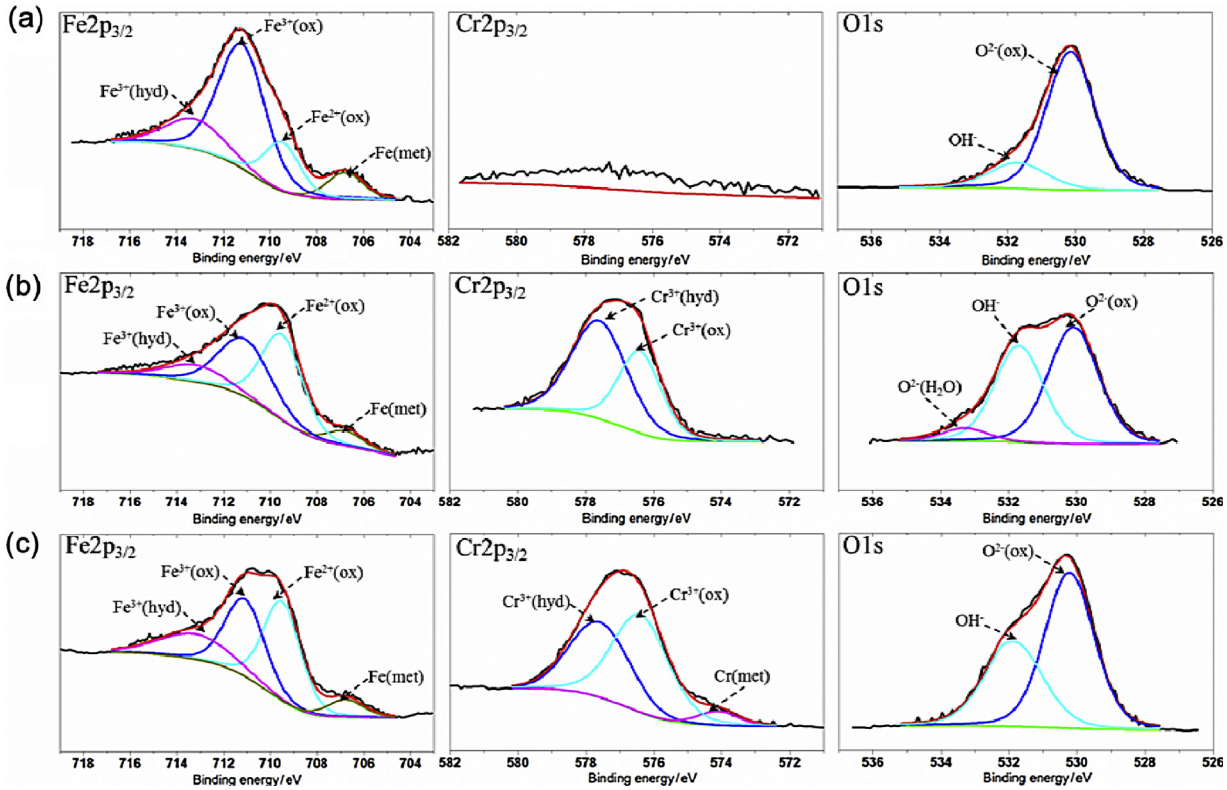

Fig. 8. XPS spectra Fe2p3/2, Cr2p3/2and O1s detected for the passive films formed on iron: (a) initial pH 8 and Cr(VI) = 52 mg L^{-1}, (b) initial pH 4 and Cr(VI) = 520 mg L^{-1} (c) initial pH 4 and Cr(VI) = 520 mg L^{-1} with T_{APC} = 10 s. The value of binding energy is before calibration.

"defect-formed" film, which led to the dissolution of iron. For T_{APC} = 10 s, peak III was not observed, implying that the film formed by a short T_{APC} was inherently more stable and protective [41,48]. Consequently, this study assumed that this finding might be relevant to the structure of passive films. X-ray photoelectron spectroscopy (XPS) experiments were conducted to investigate the structural features of passive film formed during the CV experiments.

3.4. XPS analyses

XPS analyses were performed for passive films formed on conditions of low pH, high Cr(VI) concentration and short T_{APC} strategy, respectively. The results (Fig. 8) of the analyses showed that, regardless of the conditions of formation, the species of passive films were mainly composed of Fe, Cr oxides, and hydroxides. The XPS depth profiles of the passive film revealed that high Cr(VI) concentration resulted in a thicker film (about 8 and 10 nm in pH 4 and Cr(VI) = 520 mg L^{-1} and pH 4 and Cr (VI) = 520 mg L^{-1} with T_{APC} 10 s, respectively) compared with that (about 5 nm) in low Cr(VI) concentration (pH 8 and Cr(VI) = 52 mg L^{-1}).

The ratios of Cr/(Cr + Fe), Cr^{3+}(ox)/Cr, $Fe^{3+}/(Fe^{3+} + Fe^{2+})$, and $O^{2-}/(O^{2-} + OH^{-})$ in the oxide layer for every 50 s depth were calculated based on the results of the chemical composition and depth analyses; the measurements are shown in Fig. 9. An important decrease of the content of Cr species was observed for films formed in pH 8 and Cr(VI) = 52 mg L^{-1} comparative to the films formed in pH 4 and Cr(VI) = 520 mg L^{-1}. In fact, the films in the former case essentially contained Fe species ($Fe^{3+}/(Fe^{3+} + Fe^{2+})$ 71.0%) but negligible levels of Cr (Cr/(Cr + Fe) 1.2%), whereas the films in the latter case were composed of a larger amount of Cr(Cr/(Cr + Fe) 39.7%). This trend indicates, again, that the film formed in pH 4 and Cr(VI) = 520 mg L^{-1} was more stable than that in pH 8 and Cr (VI) = 52 mg L^{-1}. Moreover, the film formed with short T_{APC} strategy displayed the highest concentration of Cr(Cr/(Cr + Fe) 48%) and litter fluctuant (std = 6.14) of chemical composition for each depth, suggesting that a uniform construction was formed and exhibited the most stable characteristic among the three cases.

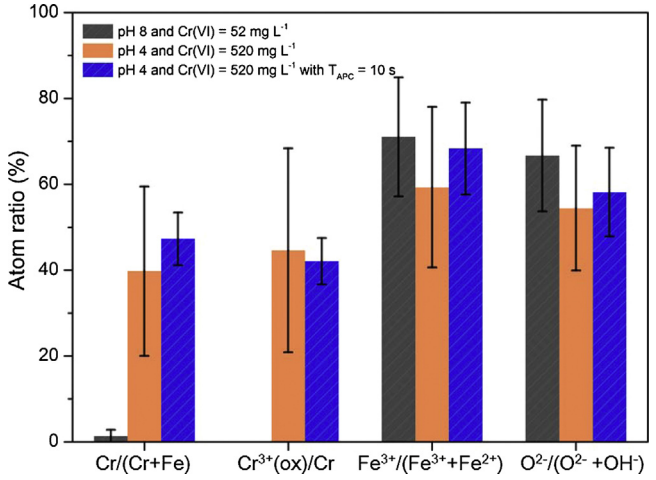

Fig. 9. Evolution of the ratios: Cr/(Cr + Fe); Cr^{3+}(ox)/Cr; $Fe^{3+}/(Fe^{3+} + Fe^{2+})$ and $O^{2-}/(O^{2-} + OH^{-})$ presented in the film calculated from the XPS spectra at different conditions: initial pH 8 and Cr(VI) = 52 mg L^{-1}, initial pH 4 and Cr(VI) = 520 mg L^{-1}, initial pH 4 and Cr(VI) = 520 mg L^{-1} with T_{APC} = 10 s.

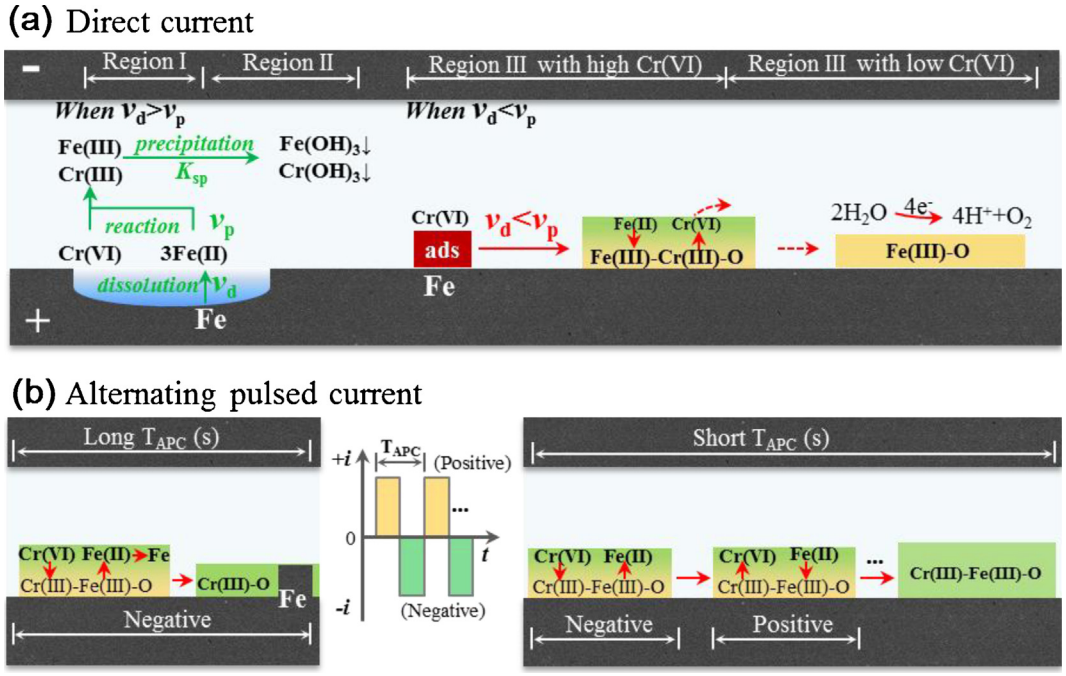

Fig. 10. Schematic illustration of the behavior of dissolution/passivation and the transformation of passive films during EC process.

3.5. Behavior of dissolution/passivation and transformation of passive films

As summarized in Fig. 10a, the solution pH in Region I was very low, which eventually resulted in $v_d > v_p$. This finding clarifies that passivation did not occur. Low pH favored the reduction of Cr(VI) to Cr(III) (Eq. (3)) [28]; yet, it significantly inhibited the Cr(III) precipitation (Eq. (7)) because the final pH (the pH that corresponded to the Cr(VI) completely reduced to Cr(VI)) was acidic. Similar to the case in Region I, no passivation occurred in Region II, from which an alkaline final pH was obtained. This pH favored the precipitation of Cr(III). Thus, Region II was considered the optimal conditions for EC operation.

Compared with Regions I and II, Region III had an increase in solution pH that decreased the dissolution rate (Eq. (2)). By contrary, the Cr(VI) gathered to the surrounding of anode under the applied electric field with high Cr(VI), thereby significantly increasing the precipitation rate (Eq. (5 to 7)). Therefore, the precipitation rate surpassed the dissolution rate, and the passivation occurred. When the passive film formed on the surface of iron electrode, it induced an increase in the potential of anode, transforming Fe(II) to Fe(III) (Eq. (14)). Subsequently, the Cr(III) species were dissolved (Eq. (17)) when the potential continued to attain the chromate oxidation potential. However, the stability of passive film formed in low Cr(VI) was less than that in high Cr(VI), resulting in more Cr(III) loss and a thinner passive film. Accordingly, such potential could ultimately increase to the potential of oxygen evolution, thereby decreasing the current efficiency.

When the polarity reversed to negative (Fig. 10b), the Cr(VI) transformed to Cr(III) (reverse of Eq. (17)), and the Fe(III) was converted to Fe(II) (Eqs. (10 to 11)). If the reaction time was sufficiently longer, the Fe(II) would ultimately reduce to Fe^0. Thus, the passive film formed in long T_{APC} was in a non-protective and "defect-formed" film state. However, under short T_{APC} condition, the reduction of metallic oxides/hydroxides was a continuous and reversible process that produced a thicker passive film with higher amounts of Cr and Fe oxides. In this process, a uniform structure was obtained and the stability of the film was improved.

4. Conclusions

This study demonstrated that the current efficiency was influenced by initial pH, Cr(VI) concentration, and APC rather than by current density. The interaction term of the initial pH-Cr (VI) concentration significantly affected passivation.

Thus, a dissolution/passivation region diagram with different initial pH and Cr(VI) concentration was constructed. The diagram showed that the dissolution Region I ($v_d > v_p$) favored the reduction of Cr(VI) to Cr(III); yet, it significantly inhibited the Cr(III) precipitation. The dissolution Region II ($v_d > v_p$) contained the optimal conditions for EC operation because it achieved a reasonable final pH for precipitation and did not suffer passivation.

In the passivation Region III ($v_d < v_p$), the stabilities of the passive film were as follows: pH 8 and Cr(VI) = 520 mg L^{-1} > pH 4 and Cr(VI) = 520 mg L ultimately[1] > pH 8 and Cr(VI) = 52 mg L^{-1} ultimately. The findings of the experiments further signified that the passive film obtained under low Cr(VI) conditions (pH 4 and Cr (VI) = 52 mg L^{-1}) essentially contained Fe species ($Fe^{3+}/(Fe^{3+} + Fe^{2+})$ 71.0%) but negligible levels of Cr (Cr/Cr + Fe only 1.2%), whereas the films under high Cr(VI) conditions (pH 8 and Cr(VI) = 520 mg L^{-1}) was rich in Cr(Cr/(Cr + Fe) 39.7%)

Depassivation was achieved by forming a non-protective passive film when it was subjected to the long period of APC (T_{APC} = 590 s), but became more stable at the short period of APC (T_{APC} = 10 s). Based on the above results, the behavior of dissolution/passivation and the transformation of passive films during the Fe-EC process were elucidated.

Acknowledgements

We are grateful for the National Key Science and Technology Project for Water Environmental Pollution Control (2009ZX07212-

001-02), the financial support of the National Natural Science Foundation of China (51378198).

References

[1] P. Gao, X.M. Chen, F. Shen, G.H. Chen, Removal of chromium(VI) from wastewater by combined electrocoagulation-electroflotation without a filter, Sep. Purif. Technol. 43 (2005) 117–123.
[2] I. Heidmann, W. Calmano, Removal of Cr(VI) from model wastewaters by electrocoagulation with Fe electrodes, Sep. Purif. Technol. 61 (2008) 15–21.
[3] M.G. Arroyo, V. Perez-Herranz, M.T. Montanes, J. Garcia-Anton, J.L. Guinon, Effect of pH and chloride concentration on the removal of hexavalent chromium in a batch electrocoagulation reactor, J. Hazard. Mater. 169 (2009) 1127–1133.
[4] X. Chen, G. Chen, Electroflotation, in: C. Comninellis, G. Chen (Eds.), Electrochemistry for the Environment, Springer, New York, 2010, pp. 263–277.
[5] H.Y. Xu, Z.H. Yang, G.M. Zeng, Y.L. Luo, J. Huang, L.K. Wang, P.P. Song, X. Mo, Investigation of pH evolution with Cr(VI) removal in electrocoagulation process: Proposing a real-time control strategy, Chem. Eng. J. 239 (2014) 132–140.
[6] M. Kobya, U. Gebologlu, F. Ulu, S. Oncel, E. Demirbas, Removal of arsenic from drinking water by the electrocoagulation using Fe and Al electrodes, Electrochim. Acta 56 (2011) 5060–5070.
[7] S. Cotillas, J., Llanos, O.G., Miranda, G.C. Díaz-Trujillo, P. Cañizares, M.A. Rodrigo, Coupling UV irradiation and electrocoagulation for reclamation of urban wastewater, Electrochim. Acta.
[8] P. Lakshmipathiraj, G.B. Raju, M.R. Basariya, S. Parvathy, S. Prabhakar, Removal of Cr (VI) by electrochemical reduction, Sep. Purif. Technol. 60 (2008) 96–102.
[9] H. Sarahney, X. Mao, A.N. Alshawabkeh, The role of iron anode oxidation on transformation of chromium by electrolysis, Electrochim. Acta 86 (2012) 96–101.
[10] C. Phalakornkule, P. Sukkasem, C. Mutchimsattha, Hydrogen recovery from the electrocoagulation treatment of dye-containing wastewater, Int. J. Hydrogen Energy 35 (2010) 10934–10943.
[11] E. Ali, Z. Yaakob, Electrocoagulation for Treatment of Industrial Effluents and Hydrogen Production, Edited by Janis Kleperis and Vladimir Linkov (2012); 227
[12] S. Aber, A.R. Amani-Ghadim, V. Mirzajani, Removal of Cr(VI) from polluted solutions by electrocoagulation: Modeling of experimental results using artificial neural network, J. Hazard. Mater. 171 (2009) 484–490.
[13] X. Chen, G. Chen, P.L. Yue, Investigation on the electrolysis voltage of electrocoagulation, Chem. Eng. Sci. 57 (2002) 2449–2455.
[14] M.Y.A. Mollah, R. Schennach, J.R. Parga, D.L. Cocke, Electrocoagulation (EC) – science and applications, J. Hazard. Mater. 84 (2001) 29–41.
[15] S. Verma, V. Khandegar, A. Saroha, Removal of Chromium from Electroplating Industry Effluent Using Electrocoagulation, Journal of Hazardous, Toxic, and Radioactive Waste 17 (2013) 146–152.
[16] E. Keshmirizadeh, S. Yousefi, M.K. Rofouei, An investigation on the new operational parameter effective in Cr(VI) removal efficiency: A study on electrocoagulation by alternating pulse current, J. Hazard. Mater. 190 (2011) 119–124.
[17] M. Stratmann, J. Müller, The mechanism of the oxygen reduction on rust-covered metal substrates, Corros. Sci. 36 (1994) 327–359.
[18] N. Sato, Basics of Corrosion Chemistry, Green Corrosion Chemistry and Engineering: Opportunities and Challenges, (2012) 1–32.
[19] M. Cohen, THE FORMATION AND PROPERTIES OF PASSIVE FILMS ON IRON, Can. J. Chem. 37 (1959) 286–291.
[20] M. Cohen, Thin Oxide Films on Iron, J. Electrochem. Soc. 121 (1974) 191C–197C.
[21] N. Sato, 1989 Whitney Award Lecture: Toward a More Fundamental Understanding of Corrosion Processes, Corrosion 45 (1989) 354–368.
[22] M. Nordsveen, S. Nešić, R. Nyborg, A. Stangeland, A Mechanistic Model for Carbon Dioxide Corrosion of Mild Steel in the Presence of Protective Iron Carbonate Films—Part 1: Theory and Verification, Corrosion 59 (2003) 443–456.
[23] S. Nešić, K.L.J. Lee, A Mechanistic Model for Carbon Dioxide Corrosion of Mild Steel in the Presence of Protective Iron Carbonate Films—Part 3: Film Growth Model, Corrosion 59 (2003) 616–628.
[24] S. Nešić, Key issues related to modelling of internal corrosion of oil and gas pipelines – A review, Corros. Sci. 49 (2007) 4308–4338.
[25] C. Noubactep, A. Schöner, Metallic iron for environmental remediation: Learning from electrocoagulation, J. Hazard. Mater. 175 (2010) 1075–1080.
[26] P. Cañizares, C. Jiménez, F. Martínez, C. Sáez, M.A. Rodrigo, Study of the Electrocoagulation Process Using Aluminum and Iron Electrodes, Ind. Eng. Chem. Res. 46 (2007) 6189–6195.
[27] I. Heidmann, W. Calmano, Removal of Ni, Cu and Cr from a galvanic wastewater in an electrocoagulation system with Fe- and Al-electrodes, Sep. Purif. Technol. 71 (2010) 308–314.
[28] I.J. Buerge, S.J. Hug, Kinetics and pH dependence of chromium(VI) reduction by iron(II), Environ. Sci. Technol. 31 (1997) 1426–1432.
[29] J.P. Gould, The kinetics of hexavalent chromium reduction by metallic iron, Water Res. 16 (1982) 871–877.
[30] A.K. Golder, A.K. Chanda, A.N. Samanta, S. Ray, Removal of hexavalent chromium by electrochemical reduction-precipitation: Investigation of process performance and reaction stoichiometry, Sep. Purif. Technol. 76 (2011) 345–350.
[31] M. Eyvaz, M. Kirlaroglu, T.S. Aktas, E. Yuksel, The effects of alternating current electrocoagulation on dye removal from aqueous solutions, Chem. Eng. J. 153 (2009) 16–22.
[32] G. Chen, Electrochemical technologies in wastewater treatment, Sep. Purif. Technol. 38 (2004) 11–41.
[33] P. Schmuki, H. Böhni, F. Mansfeld, A Photoelectrochemical Investigation of Passive Films Formed by Alternating Voltage Passivation, J. Electrochem. Soc. 140 (1993) L119–L121.
[34] S. Fujimoto, K. Tsujino, T. Shibata, Growth and properties of Cr-rich thick and porous oxide films on Type 304 stainless steel formed by square wave potential pulse polarisation, Electrochim. Acta 47 (2001) 543–551.
[35] J. Huang, Z.H. Yang, G.M. Zeng, M. Ruan, H.Y. Xu, W.C. Gao, Y.L. Luo, H.M. Xie, Influence of composite flocculant of PAC and MBFGA1 on residual aluminum species distribution, Chem. Eng. J. 191 (2012) 269–277.
[36] C.-Y. Hu, S.-L. Lo, Y.-H. Liou, Y.-W. Hsu, K. Shih, C.-J. Lin, Hexavalent chromium removal from near natural water by copper–iron bimetallic particles, Water Res. 44 (2010) 3101–3108.
[37] M.H. Isa, E.H. Ezechi, Z. Ahmed, S.F. Magram, S.R.M. Kutty, Boron removal by electrocoagulation and recovery, Water Res. 51 (2014) 113–123.
[38] A. Mahmoud, A.F.A. Hoadley, An evaluation of a hybrid ion exchange electrodialysis process in the recovery of heavy metals from simulated dilute industrial wastewater, Water Res. 46 (2012) 3364–3376.
[39] G. Mouedhen, M. Feki, M. De Petris-Wery, H.F. Ayedi, Electrochemical removal of Cr(VI) from aqueous media using iron and aluminum as electrode materials: Towards a better understanding of the involved phenomena, J. Hazard. Mater. 168 (2009) 983–991.
[40] Y.F. Cheng, J.L. Luo, Passivity and pitting of carbon steel in chromate solutions, Electrochim. Acta 44 (1999) 4795–4804.
[41] S. Virtanen, M. Büchler, Electrochemical behavior of surface films formed on Fe in chromate solutions, Corros. Sci. 45 (2003) 1405–1419.
[42] I. Díez-Pérez, P. Gorostiza, F. Sanz, C. Müller, First Stages of Electrochemical Growth of the Passive Film on Iron, J. Electrochem. Soc. 148 (2001) B307–B313.
[43] L. Wang, K. Daub, Z. Qin, J.C. Wren, Effect of dissolved ferrous iron on oxide film formation on carbon steel, Electrochim. Acta 76 (2012) 208–217.
[44] L. Freire, M.A. Catarino, M.I. Godinho, M.J. Ferreira, M.G.S. Ferreira, A.M.P. Simoes, M.F. Montemor, Electrochemical and analytical investigation of passive films formed on stainless steels in alkaline media, Cem. Concr. Compos. 34 (2012) 1075–1081.
[45] A. Kocijan, C. Donik, M. Jenko, Electrochemical and XPS studies of the passive film formed on stainless steels in borate buffer and chloride solutions, Corros. Sci. 49 (2007) 2083–2098.
[46] I.B. Singh, D.R. Singh, Effects of pH on Cr-Fe interaction during Cr(VI) removal by metallic iron, Environ. Technol. 24 (2003) 1041–1047.
[47] Y.F. Cheng, J.L. Luo, A comparison of the pitting susceptibility and semiconducting properties of the passive films on carbon steel in chromate and bicarbonate solutions, Appl. Surf. Sci. 167 (2000) 113–121.
[48] H. He, T. Zhang, C. Zhao, K. Hou, G. Meng, Y. Shao, F. Wang, Effect of alternating voltage passivation on the corrosion resistance of duplex stainless steel, J. Appl. Electrochem. 39 (2009) 737–745.